

Measuring Directionality in Double Beta Decay and Neutrino Interactions with Kiloton-Scale Scintillation Detectors

C. Aberle,¹ A. Elagin,² M. Wetstein,² H. J. Frisch,² and L. Winslow¹

¹*University of California Los Angeles, Los Angeles, CA 90095, USA*

²*University of Chicago, Chicago, IL 60637, USA*

(Dated: July 21, 2013)

Large liquid-scintillator-based detectors have proven to be exceptionally effective for low energy neutrino measurements due to their good energy resolution and scalability to large volumes. The addition of directional information using Cherenkov light and fast timing would enhance the scientific reach of these detectors, especially for searches for neutrino-less double-beta decay. In this paper, we develop a technique for extracting particle direction using the difference in arrival times for Cherenkov and scintillation light, and evaluate several detector advances in timing, photodetector spectral response, and scintillator emission spectra that could be used to make direction reconstruction a reality in a kiloton-scale detector.

PACS numbers: 23.40.-s, 21.10.Tg, 14.60.Pq, 27.60.+j

I. INTRODUCTION

Liquid scintillator based detectors are responsible for several of the critical measurements that have determined our present understanding of neutrino masses and mixings. These measurements include KamLAND's measurement of reactor anti-neutrino oscillation at a distance of ~ 200 km[1], Borexino's measurement of ^7Be solar neutrino oscillation[2], and most recently the short baseline reactor anti-neutrino experiments that measured oscillations due to θ_{13} at a distance of 1 km: Daya Bay[3], Double Chooz[4, 5], and RENO[6]. Scintillator-based neutrino detectors will continue to be important for the next set of neutrino measurements, from the determination of the neutrino mass hierarchy[7, 8] to elastic scattering measurements[9] and sterile neutrino searches[10, 11], and for non-proliferation applications[12, 13].

The scalability of these detectors to large volumes also makes them highly competitive for neutrino-less double-beta ($0\nu\beta\beta$) decay searches in which the final state consists of a pair of electrons with energies in the few MeV range. The observation of this rare decay would prove that the neutrino is a Majorana particle, which has profound consequences to our understanding of the generation of mass and may provide a possible explanation of the matter-antimatter asymmetry in the universe. Currently one of the best limits for the $0\nu\beta\beta$ half-life comes from the scintillating detector KamLAND-Zen[14].

The advantage of liquid scintillators for measurements in the ~ 1 MeV range is their scalability from 1 ton to 1 kiloton while providing energy resolutions of $\sim 5\%$. This is roughly a factor of two better than water Cherenkov detectors, the other developed technology that can be economically scaled to these large masses. However, for scintillator-based detectors, while the energy resolution is good due to the abundance of light, the light is isotropic and does not retain the directional information of the primary particle. In contrast, the direction of the particle can be reconstructed from the Cherenkov cone in water-based detectors, although the energy resolution rapidly degrades below ~ 5 MeV. For double-beta decay in particular, but also for neutrino interactions, the directional information

can be a strong suppressant of backgrounds.

In a liquid-scintillation-based detector, Cherenkov light is also produced, although most is absorbed and re-emitted as part of the scintillation processes. However, some fraction retains its directional information. If this directional Cherenkov light can be isolated from the copious isotropic scintillation light, it may be possible to reconstruct the direction of the primary particle or, in the case of double beta decay, to determine the existence and topology of the pair. The addition of directionality is thus a powerful tool for background rejection. In this paper, we develop a technique for separating the Cherenkov and scintillation light using the photon arrival times and evaluate several detector technologies that would allow the realization of direction reconstruction in kilo-ton scale scintillating neutrino detectors.

II. LIQUID SCINTILLATOR DETECTORS

Liquid scintillators are 'cocktails' of aromatic hydrocarbons. When charged particles move through a scintillator, the molecules are excited, predominantly via the non-localized electrons in the π -bonds of the phenyl groups [15]. Vibrational and rotational modes of the molecules are turned into heat within picoseconds through collisions with other molecules. Within ~ 10 picoseconds, the π -electrons de-excite to the first excited state from higher levels through radiation-less transitions. The first excited state de-excites through photon emission. There are two characteristic times for this de-excitation, depending if the singlet state or the triplet state was excited. The singlet state will de-excite within nanoseconds while the triplet state de-excites on the order of 10's or 100's of nanoseconds. These two processes are fluorescence and phosphorescence respectively. The exact time constants for these processes are determined by the composition of the scintillator.

The absorption and emission spectra overlap at some level in all molecules. Consequently, if there is only one type of molecule in the scintillator cocktail the light output is reduced due to inefficiencies in the energy transfer through multiple

absorption and re-emission processes. Aromatic solutes or fluors are added to the primary solvent to shift the wavelength of the photons to longer wavelengths where the scintillator is more transparent. This wavelength-shifting is also used to match the quantum efficiency as a function of wavelength for the photodetectors being used. One typical scintillator mixture uses pseudo-cumene as the solvent with 1-5 g/L of PPO as the fluor. This mixture has a peak emission at about 400 nm where bi-alkali photomultiplier tubes (PMTs) are most sensitive and the pseudo-cumene is relatively transparent.

A good liquid scintillator will produce $\sim 10,000$ photons isotropically per MeV of deposited energy. Although less abundant, Cherenkov light will be produced as well if a particle is moving faster than the speed of light in the medium. This light is emitted in a cone centered on the direction of the particle trajectory, and with a continuous spectrum weighted toward shorter wavelengths but extending well into the red. The spectrum is described by [16]:

$$\frac{dN}{d\lambda dx} = \frac{2\pi\alpha Z^2}{\lambda^2} \left[1 - \frac{1}{\beta^2 n(\lambda)^2} \right] \quad (1)$$

where $n(\lambda)$ is the wavelength-dependent index of refraction and β is the velocity of the incoming particle. In a large detector, the Cherenkov light produced at wavelengths shorter than the absorption cutoff of the scintillator will be absorbed and re-emitted as isotropic light, but wavelengths longer than this cutoff will propagate across the detector, retaining their directional information. The yield is roughly 60 photons per MeV, assuming a 400 nm absorption cutoff [17]. These undisturbed Cherenkov photons will have timing determined by the group velocity [18] in the liquid,

$$v_g(\lambda) = \frac{c_{vacuum}}{n(\lambda) - dn(\lambda)/d\log(\lambda)}. \quad (2)$$

The longer wavelength Cherenkov photons typically arrive before the scintillation light, which is slowed by both the scintillation processes and the shorter wavelengths involved. Thus, with sufficient timing resolution and sensitivity to longer wavelengths it should be possible to separate the directional Cherenkov light and the isotropic scintillation light, and then to reconstruct the direction of the initial particle.

In $0\nu\beta\beta$, the electrons emerge with a combined energy equal to the Q -value of the particular isotope. The individual electrons come out following distributions of energies and angular correlations, a probable case being equal division of energy between back-to-back electrons [19]. This case is shown in FIG. 1 for an example ^{116}Cd $0\nu\beta\beta$ event. Since the decay half-life is inversely proportional to the phase-space factor, isotopes with higher Q -values are preferred and due to backgrounds from the daughters of the ^{238}U and ^{232}Th decay chains those with Q -values at or above 2.6 MeV are most often considered for $0\nu\beta\beta$ searches. There are hundreds of candidate $0\nu\beta\beta$ isotopes [20], but only a handful with large Q -values. Most of the high Q -value candidates have been considered as a dopant for a liquid scintillator: ^{150}Nd ($Q=3.367$ MeV) [21], ^{144}Nd ($Q=3.350$ MeV) [17], ^{116}Cd ($Q=2.802$ MeV) [17, 25], ^{130}Te ($Q=2.533$ MeV) [17, 26], ^{136}Xe ($Q=2.479$ MeV) [14] and ^{124}Sn ($Q=2.29$ MeV) [27]. Xenon gas readily dissolves into liquid scintillator. For the other isotopes, suitable organometallic compound needs to be found that produces a stable scintillator with a long attenuation length in the wavelength region of interest. Recently, nanocrystals called quantum dots have been explored as an alternative method for doping scintillator [17, 28]. Quantum dots have interesting optical properties which are discussed further in Section VI.

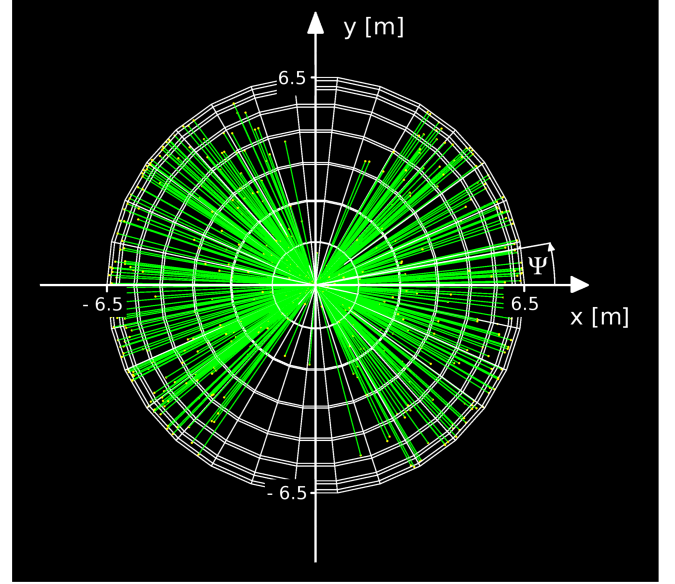


FIG. 1: Two back-to-back electrons with 1.41 MeV each (equally divided energy of ^{116}Cd $0\nu\beta\beta$ decay) at the center of the sphere with initial directions along the x and $-x$ -axis. Only Cherenkov photons (green lines) are drawn to illustrate the directionality of the event.

^{82}Se ($Q=3.350$ MeV) [17], ^{116}Cd ($Q=2.802$ MeV) [17, 25], ^{130}Te ($Q=2.533$ MeV) [17, 26], ^{136}Xe ($Q=2.479$ MeV) [14] and ^{124}Sn ($Q=2.29$ MeV) [27]. Xenon gas readily dissolves into liquid scintillator. For the other isotopes, suitable organometallic compound needs to be found that produces a stable scintillator with a long attenuation length in the wavelength region of interest. Recently, nanocrystals called quantum dots have been explored as an alternative method for doping scintillator [17, 28]. Quantum dots have interesting optical properties which are discussed further in Section VI.

The reconstruction of the direction of the two simultaneous emitted ~ 1.5 MeV electrons from the $0\nu\beta\beta$ decay is quite challenging. In this paper, we decided to start our directional studies with 5 MeV single electrons since reconstruction of direction in this energy range had never been achieved. This is a logical energy to use since this is where historically scintillating detectors become more practical than water Cherenkov detectors. This is also an energy that is relevant for studies of ^8B solar neutrinos and neutrino-electron elastic scattering measurement.

III. GEANT4 SIMULATION

In order to study the effects relevant to directional reconstruction in liquid scintillators, a GEANT4 [29, 30] simulation has been constructed. The simulation uses GEANT4 Version 4.9.6 with the default liquid scintillator optical model, in which optical photons are assigned the group velocity in the wavelength region of normal dispersion.

The detector geometry is a sphere of 6.5 m radius filled with scintillator. FIG. 1 shows the geometry and the

Cherenkov light from an example $^{116}\text{Cd } 0\nu\beta\beta$ event. The default scintillator properties have been chosen to match the KamLAND scintillator [31]: 80% n-Dodecane, 20% Pseudocumene (1,2,4-Trimethylbenzene) and 1.52 g/l PPO (2,5-Diphenyloxazole). The scintillator properties implemented in the simulation include the atomic composition and density ($\rho = 0.78$ g/ml), the wavelength-dependent attenuation length [32] and refractive index [33], the scintillation emission spectrum [32], emission rise time ($\tau_r = 1.0$ ns) and emission decay time constants ($\tau_{d1} = 6.9$ ns and $\tau_{d2} = 8.8$ ns) with relative weights of 0.87 and 0.13 [34], scintillator light yield (LY, 9030 photons/MeV) and the Birks constant ($k_B \approx 0.1$ mm/MeV) [35]. Variations from the baseline KamLAND case are discussed below. Re-emission of absorbed photons in the scintillator bulk volume and scattering have not yet been included, but are not expected to change the conclusions here.

The inner sphere surface is used as the photodetector. It is treated as fully absorbing (no reflections), with a photodetector coverage of 100%. Two important photodetector properties have been varied: 1) the transit time spread (TTS, default $\sigma = 0.1$ ns) and 2) the wavelength-dependent quantum efficiency (QE) for photoelectron production. The default is the QE of a bialkali photocathode (Hamamatsu R7081 PMT) [36], for which digitized values come from the Double Chooz [4] Monte Carlo simulation. We note that the KamLAND 17-inch PMTs use the same photocathode type with similar quantum efficiency.

Before the simulation results for different simulation settings are discussed, we note that we concentrate on 5 MeV single electrons since this is the energy at which scintillating detectors become more practical than water Cherenkov detectors. We now highlight the effects which contribute to the timing of the scintillator detector system. First, the simulated travel time of the initial 5 MeV electron is between 0.10 and 0.15 ns, while the travel distance is about 3 cm. Second, the scintillation light emission follows a distribution characterized by scintillator-specific rise and decay times. Before the solutes in liquid scintillator can emit optical photons, the energy has to be transferred from the solvent to the solute. The time constant of this energy transfer accounts for a rise time in scintillation light emission. Past neutrino experiments were not highly sensitive to the effect of the scintillation rise time, which is the reason why there is a lack of accurate numbers. We assume a rise time of 1.0 ns; more detailed studies are needed in the future. The two time constants used to describe the falling edge of the scintillator emission time distribution (quoted above) are values specific to the KamLAND scintillator. Third, chromatic dispersion turns out to be an important effect in a 6.5m-radius detector at the level of precision needed for direction reconstruction.

Due to the wavelength-dependence of the refractive index the speed of light in the scintillator (see Equation (2)) increases with increasing photon wavelengths for normal dispersion, with red light traveling faster than blue light. In order to study the measurability of the time differences, we simulated 5 MeV electrons at the center of the sphere where we used instantaneous scintillation emission with the quantum efficiency applied, but not including a transit-time spread. The

true hit time distributions of photoelectrons were analyzed for scintillation light and Cherenkov light separately. Photoelectrons coming from Cherenkov light are on average created about 0.5 ns earlier than PEs from scintillation light. The RMS values from PE time distributions for Cherenkov and scintillation light are both about 0.5 ns. Note that these numbers include the effect of the finite electron travel time.

The measurement of the arrival times of single photoelectrons is affected by the transit-time spread (TTS) of the photodetectors, a number which can be different by orders of magnitude depending on the detector type. The default TTS of 0.1 ns (σ) is a value which can be achieved with the large area picosecond photodetectors (LAPPDs) [37, 38] and possibly hybrid photodetectors (HPDs) [39]; even significantly lower TTS numbers are realistic with the LAPPD [40–42]. We note that uncertainties in the vertex reconstruction will produce a similar effect to the smearing due to the TTS.

In Sections IV to VI, we study the photoelectron timing for different detector configurations. We focus on the idea to increase discrimination between Cherenkov and scintillation light by using improved detector timing. The primary quantities provided by the GEANT4 simulation are the photoelectron hit positions and the detection times after the TTS resolution has been applied. In Section VII these quantities are then used for event reconstruction.

IV. DETECTOR TIMING

We first discuss results for the default simulation settings described in the previous section. FIG. 2 (a) shows the TTS-smearred photoelectron (PE) detection times for 1000 simulated electrons with 5 MeV energy in the center of the detector with initial momentum directions coinciding with the x-axis. The photoelectrons induced by Cherenkov light arrive earlier, as expected due to the instantaneous emission and the higher average photon speed compared to scintillation light. There is however significant overlap of the two arrival time distributions.

In order to compare simulations with different parameters, a fixed time cut of $t \leq 34.0$ ns is applied using the truth information to isolate the Cherenkov light in this early time window. For the default simulation case, the average number of PEs per event coming from Cherenkov light in the early time window (108) is 98% of the total average number of PEs from Cherenkov light (110). For scintillation light, the average number of PEs (171) is only 3.2% of the average total scintillation-induced PEs (5445). This indicates the effectiveness of a time cut to separate Cherenkov light from scintillation light.

The ratio of Cherenkov-induced to scintillation-induced photo-electrons in the early time window ($R_{C/S}$) is a useful figure-of-merit when comparing different simulation settings, since a higher ratio means more directional information per PE. For the default simulation settings $R_{C/S} = 0.63$.

FIG. 3 displays the angular distribution of PE hits after the time cut. Although this time cut is a simplification of actual time reconstruction effects, we can use it to indicate the spatial

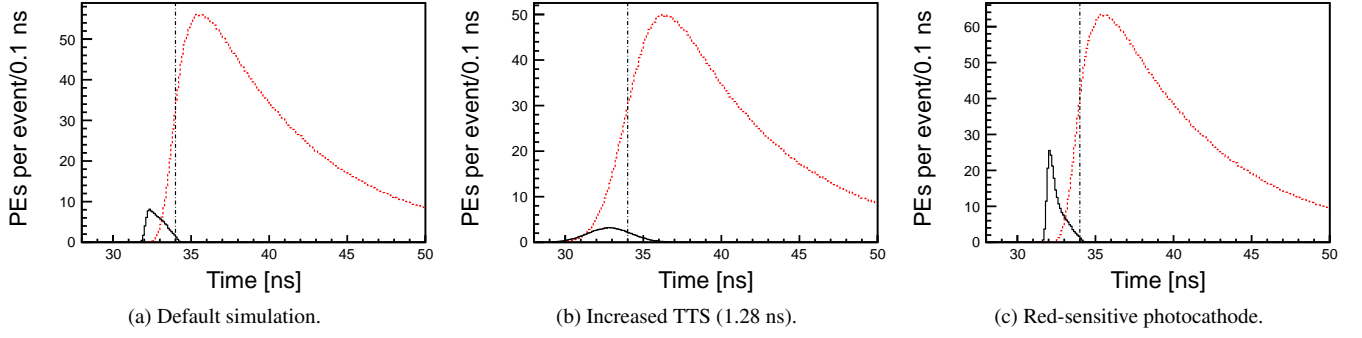


FIG. 2: Photo-electron (PE) arrival times after application of the transit-time spread (TTS) for the simulation of 1000 electrons (5 MeV) with different values of the TTS and wavelength response. PEs from Cherenkov light (black, solid line) and scintillation light (red, dotted line) are compared. The dashed vertical line illustrates a time cut at 34 ns. (a) Default simulation: bialkali photocathode and TTS = 0.1 ns (σ). After the 34.0 ns time cut we get 171 PEs from scintillation and 108 PEs from Cherenkov light. (b) Default simulation settings except for TTS = 1.28 ns (KamLAND 17 in. PMTs). After the 34.0 ns time cut we get 349 PEs from scintillation and 88 PEs from Cherenkov light. (c) Default simulation settings except for a GaAsP photocathode. After the 34.0 ns time cut we get 226 PEs from scintillation and 229 PEs from Cherenkov light.

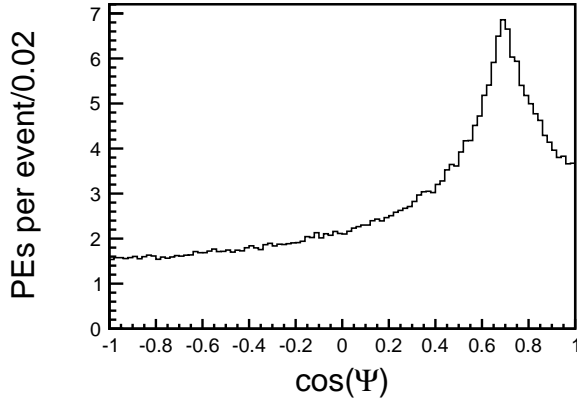


FIG. 3: The angular distribution of photoelectron hits relative to the original electron direction $\cos(\Psi) = x_{hit}/\vec{r}_{hit}$. The sample consists of 1000 events with a 5 MeV electron produced at the detector center. Default simulation settings are used and both Cherenkov and scintillation light are included.

V. DETECTOR WAVELENGTH RESPONSE

In addition to decreasing the photodetector TTS to enhance $R_{C/S}$, it is possible to optimize the wavelength-dependence of the photocathode. Since Cherenkov photons which passed through meters of scintillator have longer average wavelengths than scintillation photons, a photodetector which is more sensitive at long wavelengths increases not only the absolute number of PEs but also the ratio between Cherenkov- and scintillation-induced PEs.

We have run the simulation with the QE of an extended red-sensitive GaAsP photocathode (Hamamatsu R3809U-63) [44]. FIG. 2(c) shows the results for the modified simulation with high QE in the red spectral region. The higher absolute number of photo-electrons coming from Cherenkov light (factor of ≈ 2) and the increased Cherenkov/scintillation ratio (1.6) in the early time window would significantly improve the directionality reconstruction.

VI. SCINTILLATOR EMISSION SPECTRUM

An alternative route towards increasing the separation in time between Cherenkov and scintillation photon hits is the tuning of the scintillator emission spectrum. Recently, the use of quantum dots (QDs) in liquid scintillators has been studied as a possibility to improve future large scale neutrino experiments [28]. One major motivation for quantum-dot-doped scintillator is control of the emission spectra by tuning the size or composition of the quantum dots.

The emission spectrum of commercial alloyed core/shell $\text{CdS}_x\text{Se}_{1-x}/\text{ZnS}$ quantum dots was measured in Ref. [28]. This spectrum shows a symmetric peak centered around 461 nm with FWHM = 29 nm. In order to isolate the effect of the different emission spectrum, the other simulation settings, including the KamLAND absorption spectrum, were

distribution of hits in the early time window. The Cherenkov ring structure can be clearly seen in the peak near 46° , demonstrating that the directional signal conveyed by the Cherenkov photons is not erased by scattering of the initial 5 MeV electrons.

When the 17-inch KamLAND PMTs [32, 43] (TTS = 1.28 ns) are used in the simulation, the broadening of the time distributions leads to a strongly decreased ratio of Cherenkov over scintillation light ($R_{C/S} = 0.25$) for $t < 34$ ns (see FIG. 2 (b)). This shows that a low photodetector TTS is critical for directionality reconstruction and motivates the use of novel detector types.

kept unchanged; we find $R_{C/S} = 0.17$ for the default 34-nsec timing cut. Compared to the default case shown in FIG. 2(a) the separation is worse (as expected) because the scintillation light wavelengths are higher than in the KamLAND emission spectrum.

However, advances in the production of commercial quantum dot samples could yield quantum dots which have similar, single peak emission shapes at lower wavelengths. This case has been simulated using the same spectral shape of the measured core-shell quantum dot emission but shifted to lower wavelengths such that the emission peak is centered at 384 nm. This peak emission value has been measured for other types of QDs, however with a much more pronounced tail [28]. The resulting PE time distribution shows improved separation of Cherenkov and scintillation light compared to the default simulation. After the 34.0 ns cut on the TTS smeared PE time we obtain a Cherenkov/scintillation ratio of $R_{C/S} = 0.86$ (107 PE from Cherenkov light and 124 PE from scintillation). The number of Cherenkov-induced PEs after the time cut is unchanged while the number of PEs coming from scintillation light is decreased due to the higher average photon travel times.

VII. RECONSTRUCTION

The timing studies show that in the early time window, $t \leq 34.0$ ns, Cherenkov light dominates. In this paper, we apply reconstruction tools for a water Cherenkov detector, WCSim-Analysis, with only small modifications to remove water specific properties, to the problem of reconstructing the position and direction of 5 MeV electrons from this early light. WCSim-Analysis is a Water Cherenkov reconstruction package developed for the Long Baseline Neutrino Experiment (LBNE collaboration)[45]. It provides a framework for generic event cleaning, track reconstruction, and particle identification, and comes equipped with variety of pre-built algorithms. It is continuing to be expanded using new track-fitting techniques for Water Cherenkov detectors[46] based on advanced photosensors with sub-cm imaging capabilities and timing resolutions below 100 picoseconds[37, 38].

The results presented in this paper rely on a simple vertex reconstruction algorithm, commonly known as a “point fit”[47]. It assumes that all of the scintillation and Cherenkov light is emitted from a single point in space-time (x_0, y_0, z_0, t_0) . In actuality, the light is emitted along an extended, multi-scattered electron track. However, at the energies discussed in this paper, the extent of this track is small (a few cm) compared to the scale of the detector ($R=6.5$ meters) and thus typical photon transit distances.

The first step of the reconstruction process relies on exact numerical calculations of vertex candidates from quadruplets of hits. Given a single point source, we need four constraints to solve for the four unknowns of the vertex (x, y, z, t_0) [48]. This approach would provide an exact solution in the case of four prompt, un-scattered photons originating from a common point. However, many of these randomly chosen quadruplets will produce anomalous solutions due to ‘real world’ effects

such as delayed emission and deviations from the point-like geometry. Nonetheless, we found that any chosen subset of 400 quadruplets was a sufficiently large ensemble to assure that some solutions will be close to the true vertex.

Once a set of vertex candidates has been found, we test the goodness of each vertex and select the one that best fits the full ensemble of photon hits. The goodness of fit is determined based on the distribution of an observable known as the “point time residual”[47]. The point time residual is calculated by taking the difference between the measured time of a photon hit, and the predicted time of the hit, given its distance from the vertex hypothesis, a single effective speed of light in the scintillator, and the hypothesized t_0 of the event. The width of the time residual distribution over all hits is minimized when the hypothesized vertex is near the true vertex. Based on this figure of merit, we select the vertex with the narrowest time residual distribution from among the 400 candidates.

The direction of the electron track is then determined by taking the centroid of all vectors pointing from the fitted vertex to the hits on the detector. Since the Cherenkov light is highly directional, and since the timing cut enhances the purity of the Cherenkov light in the sample, this calculation provides a good measure of the track direction.

For the purpose of testing the reconstruction algorithm we use 1000 simulated electrons with an energy of 5 MeV. The electrons are simulated at the center of the detector, $\vec{r} = (0,0,0)$, along the x-axis, $\frac{\vec{p}}{|\vec{p}|} = (1,0,0)$. FIG. 4 shows the vertex reconstruction. The vertex is reasonably well reconstructed around the center of the detector, $\vec{r} = (0,0,0)$, except along the x-axis. The RMS values of the distributions for all three reconstructed coordinates are smaller than 3.5 cm. The shift along the x-axis is partially attributed to the untuned effective speed of light and partially to the fact that electron is moving towards that direction and has a finite track length while the reconstruction algorithm treats all photons as they were emitted from the same point. The reconstruction of the direction also is shown in Fig. 4. It shows that for the majority of the events the initial electron direction is reconstructed well. This is a very promising result given the simplicity of the algorithms used.

VIII. CONCLUSIONS

The ability to reconstruct direction in kiloton-scale scintillation detectors would be a major technological advance for neutrino experiments, especially those also searching for $0\nu\beta\beta$. More generally, this technique could be applied wherever scintillation-based detectors are used. A GEANT4 simulation of a simple spherical detector corresponding to a kiloton of scintillator shows that timing on the order of 0.1 ns is required to separate the directional Cherenkov light from the more abundant scintillation light. This separation can be improved using photodetectors with more red sensitivity and liquid scintillators with a more narrow emission spectrum shifted to shorter wavelengths. Furthermore, simple reconstruction algorithms adapted from those for water Cherenkov detectors are able to reliably reconstruct the position and direction of

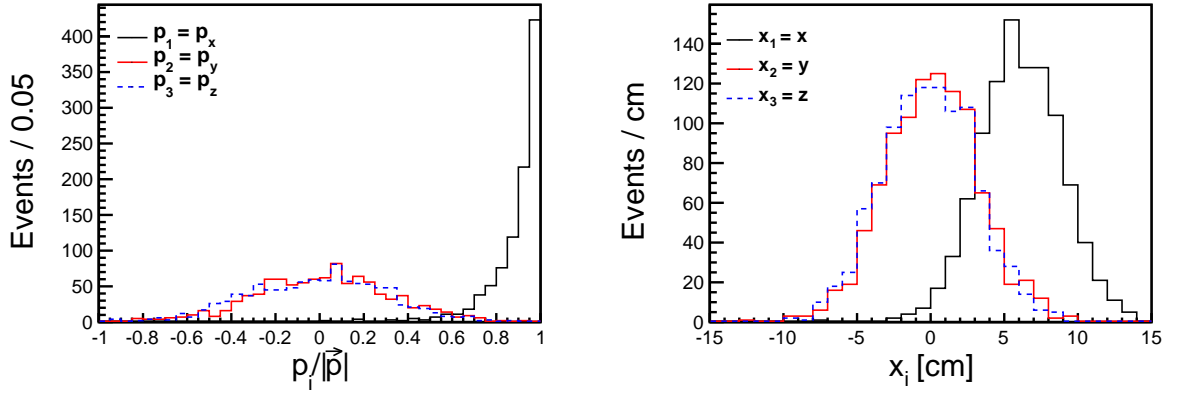


FIG. 4: (Left) The reconstructed direction, $(\frac{p_x}{|\vec{p}|}, \frac{p_y}{|\vec{p}|}, \frac{p_z}{|\vec{p}|})$, for the simulation of 1000 electrons (5 MeV). In the simulation the electrons are produced along the X-axis, $\vec{p} = (1, 0, 0)$, and originate from the center of the 6.5-m-radius detector, $\vec{r} = (0, 0, 0)$. Only photons with arrival time of $t < 34$ ns are used in the reconstruction. The quantum efficiency of the bialkali photocathode is taken into account. (Right) The reconstructed vertex position, (x, y, z) , for the same simulation.

5 MeV electrons. More detailed simulation and advanced reconstruction algorithms will need to be developed to move to lower energies and more complicated event topography, such as those in $0\nu\beta\beta$, but the technique already appears very promising.

IX. ACKNOWLEDGMENTS

The authors thank Andrew Blake at University of Cambridge for his work authoring the WCSimAnalysis code. The authors thank the neutrino reconstruction group at Iowa State, particularly Mayly Sanchez, Ioana Anghel, and Tian Xin,

for their continued work in developing the WCSimAnalysis algorithms and for their insights and expertise regarding issues related to Cherenkov reconstruction with fast-timing. The authors also thank Micheal Smy for his development of the quadruplet-based vertex-finding method. L. Winslow would like to thank J.M. Conrad for many useful discussion on the topic, and K. Arisaka for discussions on the possible reach of traditional PMTs and the characteristics of HPDs. C. Aberle and L. Winslow are supported by funds from University of California Los Angeles. The work at the University of Chicago is partially supported by DOE contract DE-SC0008172 and NSF grant PHY-1066014. Matthew Wetstein gratefully acknowledges support by the Grainger Foundation.

-
- [1] KamLAND Collaboration, A. Gando *et al.*, (2013), 1303.4667,
 - [2] Borexino Collaboration, G. Bellini *et al.*, Phys.Rev.Lett. **107**, 141302 (2011), 1104.1816.
 - [3] Daya Bay Collaboration, F. An *et al.*, Chin. Phys. **C37**, 011001 (2013), 1210.6327.
 - [4] Double Chooz Collaboration, Y. Abe *et al.*, Phys.Rev. **D86**, 052008 (2012), 1207.6632.
 - [5] Double Chooz Collaboration, Y. Abe *et al.*, Phys.Lett. **B723**, 66 (2013), 1301.2948.
 - [6] RENO Collaboration, J. K. Ahn *et al.*, Phys. Rev. Lett. **108**, 191802 (2012).
 - [7] Y.-F. Li, J. Cao, Y. Wang, and L. Zhan, (2013), 1303.6733.
 - [8] RENO-50 - International Workshop on toward Neutrino Mass Hierarchy, 2009.
 - [9] J. Conrad *et al.*, Precision $\bar{\nu}_e$ -electron Scattering Measurements with IsoDAR to Search for New Physics, In preparation, for submission to PRD., 2013.
 - [10] IsoDAR Collaboration, A. Bungau *et al.*, Phys.Rev.Lett. **109**, 141802 (2012), 1205.4419.
 - [11] K. Heeger, B. Littlejohn, and H. Mumm, (2013), 1307.2859.
 - [12] A. Porta *et al.*, Nuclear Science, IEEE Transactions on **57**, 2732 (2010).
 - [13] N. Bowden *et al.*, Nuclear Instruments and Methods in Physics Research Section A: Accelerators, Spectrometers, Detectors and Associated Equipment **572**, 985 (2007).
 - [14] KamLAND-Zen Collaboration, A. Gando *et al.*, Phys.Rev.Lett. **110**, 062502 (2013), 1211.3863.
 - [15] J.B. Birks, *The Theory and Practice of Scintillation Counting* (Pergamon Press, 1964).
 - [16] P. A. Cherenkov, Doklady Akademii Nauk SSSR **2**, 451+ (1934).
 - [17] L. Winslow and R. Simpson, Journal of Instrumentation **7**, P07010 (2012).
 - [18] A. M. Steinberg, P. G. Kwiat, and R. Y. Chiao, Phys. Rev. Lett. **68**, 2421 (1992).
 - [19] J. Kotila and F. Iachello, Phys. Rev. C **85**, 034316 (2012).
 - [20] V. Tretyak and Y. Zdesenko, Atomic Data and Nuclear Data Tables **61**, 43 (1995).
 - [21] M. Yeh, Y. Williamson, and R. L. Hahn, J.Phys.Conf.Ser. **136**, 042054 (2008).
 - [22] I. Barabanov *et al.*, Instrum.Exp.Tech. **55**, 545 (2012).
 - [23] Y. Fukuda, S. Moriyama, and I. Ogawa, Nuclear Instruments

and Methods in Physics Research Section A: Accelerators, Spectrometers, Detectors and Associated Equipment , (2013).

- [24] V. Gehman *et al.*, Nucl.Instrum.Meth. **A622**, 602 (2010), 0911.2198.
- [25] G. Bellini *et al.*, Eur.Phys.J. **C19**, 43 (2001), nucl-ex/0007012.
- [26] S. D. Biller, Phys.Rev. **D87**, 071301 (2013), 1306.5654.
- [27] KIMS Collaboration, M. Hwang *et al.*, Nucl.Instrum.Meth. **A570**, 454 (2007).
- [28] C. Aberle, J. Li, S. Weiss, and L. Winslow, (2013), 1307.4742.
- [29] GEANT4, S. Agostinelli *et al.*, Nucl.Instrum.Meth. **A506**, 250 (2003).
- [30] J. Allison *et al.*, Nuclear Science, IEEE Transactions on **53**, 270 (2006).
- [31] KamLAND Collaboration, K. Eguchi *et al.*, Phys.Rev.Lett. **90**, 021802 (2003), hep-ex/0212021.
- [32] O. Tajima, Development of liquid scintillator for a large size neutrino detector, Master's thesis, Tohoku University, 2000.
- [33] O. Perevozchikov, *Search for electron antineutrinos from the sun with KamLAND detector*, PhD thesis, University of Tennessee, 2009.
- [34] O. Tajima, *Measurement of Electron Anti-Neutrino Oscillation Parameters with a Large Volume Liquid Scintillator Detector; KamLAND*, PhD thesis, Tohoku University, 2003.
- [35] C. Grant, *A Monte Carlo Approach to ^7Be Solar Neutrino Analysis with KamLAND*, PhD thesis, University of Alabama, 2012.
- [36] Hamamatsu photonics k.k., large photocathode area photomultiplier tubes (data sheet, including r7081), 2013.
- [37] J. Anderson *et al.*, The Development of Large-Area Fast Photodetectors, 2009.
- [38] LAPPD Collaboration, Technical Design Report for the frugal MCP, 2010.
- [39] Y. Kawai, *Development of a Hybrid Photon-Detector Module for Next Generation Water-Cherenkov Detectors Yoshihiko*, PhD thesis, The Graduate University for Advanced Studies (SOKENDAI), 2007.
- [40] H. Grabas *et al.*, Nuclear Instruments and Methods in Physics Research Section A: Accelerators, Spectrometers, Detectors and Associated Equipment **711**, 124 (2013).
- [41] E. Oberla *et al.*, A 15 GSa/s, 1.5 GHz Bandwidth Waveform Digitizing ASIC, submitted to NIM A, 2013.
- [42] B. Adams *et al.*, Review of Scientific Instruments **84**, 061301 (2013).
- [43] H. Kume *et al.*, Nucl.Instrum.Meth. **205**, 443 (1983).
- [44] Hamamatsu photonics k.k., r3809u-61/-63/-64 data sheet, 2013.
- [45] A. Blake, *WCSimAnalysis Reconstruction Package*, Cavendish Laboratory, University of Cambridge, UK.
- [46] M. Sanchez and M. Wetstein, Nuclear Physics B - Proceedings Supplements **229232**, 525 (2012), Neutrino 2010.
- [47] M. Ishitsuka, *L/E Analysis of the Atmospheric Neutrino Data From Super-Kamiokande*, PhD thesis, University of Tokyo, 2004.
- [48] M. Smy, *Bonsai: Low Energy Vertex Reconstruction for DUSEL LBNE*, a talk presented to the LBNE collaboration (2010).